



Article

Monitoring Meteorological Drought in Southern China Using Remote Sensing Data

Li Liu ^{1,2,3}, Ran Huang ⁴, Jiefeng Cheng ⁵, Weiwei Liu ⁶, Yan Chen ^{1,2,3}, Qi Shao ^{1,2,3}, Dingding Duan ⁷, Pengliang Wei ^{1,2,3}, Yuanyuan Chen ⁸ and Jingfeng Huang ^{1,2,3,*} 

- ¹ Institute of Applied Remote Sensing and Information Technology, Zhejiang University, Hangzhou 310058, China; 21714122@zju.edu.cn (L.L.); chen_yan0309@zju.edu.cn (Y.C.); 11914070@zju.edu.cn (Q.S.); weipengliang@zju.edu.cn (P.W.)
- ² Key Laboratory of Agricultural Remote Sensing and Information Systems, Zhejiang University, Hangzhou 310058, China
- ³ Key Laboratory of Environment Remediation and Ecological Health, Ministry of Education, College of Natural Resources and Environmental Science, Zhejiang University, Hangzhou 310058, China
- ⁴ School of Automation, Hangzhou Dianzi University, Hangzhou 310018, China; huang@hdu.edu.cn
- ⁵ Zhejiang Geopher Spatial Planning Technology Co., Ltd., Hangzhou 310000, China; papainho@163.com
- ⁶ Department of Geography and Spatial Information Techniques, Ningbo University, Ningbo 315211, China; liuweiwei@nbu.edu.cn
- ⁷ Institute of Agricultural Resources and Regional Planning, Chinese Academy of Agricultural Sciences, Beijing 100081, China; duandingding@caas.cn
- ⁸ College of Environment, Zhejiang University of Technology, Hangzhou 310000, China; yychen91@zjut.edu.cn
- * Correspondence: hjf@zju.edu.cn; Tel.: +86-139-5717-1636



Citation: Liu, L.; Huang, R.; Cheng, J.; Liu, W.; Chen, Y.; Shao, Q.; Duan, D.; Wei, P.; Chen, Y.; Huang, J. Monitoring Meteorological Drought in Southern China Using Remote Sensing Data. *Remote Sens.* **2021**, *13*, 3858. <https://doi.org/10.3390/rs13193858>

Academic Editors: Baojie He, Ayyoob Sharifi, Chi Feng and Jun Yang

Received: 11 August 2021
Accepted: 24 September 2021
Published: 27 September 2021

Publisher's Note: MDPI stays neutral with regard to jurisdictional claims in published maps and institutional affiliations.



Copyright: © 2021 by the authors. Licensee MDPI, Basel, Switzerland. This article is an open access article distributed under the terms and conditions of the Creative Commons Attribution (CC BY) license (<https://creativecommons.org/licenses/by/4.0/>).

Abstract: Severe meteorological drought is generally considered to lead to crop damage and loss. In this study, we created a new standard value by averaging the values distributed in the middle 30–70% instead of the traditional mean value, and we proposed a new index calculation method named Normalized Indices (NI) for meteorological drought monitoring after normalized processing. The TRMM-derived precipitation data, GLDAS-derived soil moisture data, and MODIS-derived vegetation condition data from 2003 to 2019 were used, and we compared the NI with commonly used Condition Indices (CI) and Anomalies Percentage (AP). Taking the mid-to-lower reaches of the Yangtze River (MLRYR) as an example, the drought monitoring results for paddy rice and winter wheat showed that (1) NI can monitor well the relative changes in real precipitation/soil moisture/vegetation conditions in both arid and humid regions, while meteorological drought was overestimated with CI and AP, and (2) due to the monitoring results of NI, the well-known drought event that occurred in the MLRYR from August to October 2019 had a much less severe impact on vegetation than expected. In contrast, precipitation deficiency induced an increase in sunshine and adequate heat resources, which improved crop growth in 78.8% of the area. This study discusses some restrictions of CI and AP and suggests that the new NI index calculation provides better meteorological drought monitoring in the MLRYR, thus offering a new approach for future drought monitoring studies.

Keywords: meteorological drought; drought impact; paddy rice; winter wheat

1. Introduction

Drought, rainstorms, typhoons, high-temperature-induced damage, low temperature chilling injuries, and hailstorms have occurred frequently around the world in recent years. These meteorological disasters have a negative impact on normal socioeconomic development [1–4]. Drought is one of the most devastating natural disasters [5], especially in areas that rely heavily on rain-fed subsistence agriculture. Drought-induced famine seriously affects human survival and agricultural production [6–8].

After vegetation indices were developed in the 1980s, the Normalized Difference Vegetation Index (NDVI) was used to effectively monitor rainfall and drought and to estimate the impact of weather on crops and pastures in nonhomogeneous areas [9–12]. The problem is that, in addition to the weather influence, the difference in vegetation levels in these areas is also related to the differences between geographical resources (climate, soil, vegetation types, and terrain). For eliminating that portion of the NDVI, Kogan [13] calculated with Advanced Very High Resolution Radiometer (AVHRR) data the largest and lowest NDVI values during 1984–1987 for each of the 52 weeks of the year and for each pixel of Sudan. The maximum and minimum NDVI were used as the criteria for estimating the upper (favorable weather) and lower (unfavorable weather) limits of the ecosystem resources [14,15]. The difference between the maximum and minimum NDVI time series is due to weather variation. For enhancing the weather-related signal in NDVI values, the Vegetation Condition Index (VCI) was developed. The results showed that VCI was linearly positively correlated with precipitation. It was not sufficiently comprehensive to monitor drought only by the decline in NDVI, but the research proposed a generalized global meteorological disaster monitoring method based on the remote sensing index, so disaster monitoring achieved development from point to surface [16]. Similar to the VCI algorithm, various drought evaluation indexes based on different meteorological factors appeared gradually.

In 1995, the Temperature Condition Index (TCI) was developed by Kogan to estimate the maximum/minimum of the temperature envelope, which was used to determine temperature-related vegetation stress in addition to stress caused by excess rain [17]. High temperatures in the middle of the season indicate unfavorable or drought conditions, while low temperatures indicate mostly favorable conditions. Based on the Tropical Rainfall Measuring Mission (TRMM) precipitation data, Rhee et al. [18] proposed Scaled TRMM, which has the same calculation method as the VCI, while in 2013, Zhang and Jia [19] proposed the Soil Moisture Condition Index (SMCI) based on Advanced Microwave Scanning Radiometer for EOS (AMSR-E)-derived soil moisture. Over a long period of time, a variety of remote sensing drought monitoring indices have been developed for assessing meteorological drought, agricultural drought, and hydrological drought based on these Condition Indices (CI, such as VCI, TCI, PCI, and SMCI), some of which are shown in Table 1 [20–26].

The “Classification of Meteorological Drought” implemented in China on 1 November 2006, is the first national standard for monitoring meteorological drought disasters. It specifies the indicator, percentage of precipitating anomalies, which represents the changes in precipitation in a certain period compared with the average precipitation of all years. This indicator is used in daily business by the departments of the China Meteorological Administration, and it can assess monthly, seasonal, and annual drought events. The anomalies of soil moisture, vegetation, and temperature are also widely used in many studies [27–34], and they are collectively referred to as the Anomalies Percentage (AP).

Table 1. Summary of typical studies based on Condition Indices for drought monitoring.

Reference	Region and Year	Indices (Optimal Index Displayed in Bold)	Main Conclusion and Correlation between Index and Precipitation/Crop Yield
Kogan [13]	Sudan, Africa (1984–1987)	NDVI/ VCI	VCI was first proposed and was positively correlated with precipitation.
Kogan [17]	the United States (1985–1993)	VCI/TCI	TCI was first proposed; the combination of VCI and TCI was the basis for VHI.
Rhee, Im, and Carbone [18]	North Carolina/South Carolina/Arizona/New Mexico (2000–2009)	scaled LST/scaled TRMM/scaled NDVI/scaled NMDI/scaled NDWI/scaled NDDI/VHI/ SDCI /Z-Index	PCI was first proposed; SDCI performed better than existing indices such as NDVI and VHI and was positively correlated with crop yield.
Zhang and Jia [19]	Northern China (2003–2010)	PCI/SMCI/TCI/VCI/PSMCI/PTCI/SMTCI/ MIDI	SMCI was first proposed; MIDI was the optimum in monitoring short-term drought, especially for meteorological drought across northern China.
Du, et al. [35]	Shandong, China (2013–2017)	PCI/TCI/VCI/ SDI /SPI	SDI was positively correlated with precipitation and crop yield. VCI/SDI/TCI were all negatively correlated with drought affected crop area.
Zhang, et al. [36]	Hubei, Yunnan, Hebei Provinces, China (1981–2011)	PCI/SMCI/VCI/ PADI / PDSI/SPI	Compared with the correlation with precipitation, soil moisture and vegetation data alone, PADI correlated well with wheat yield loss.
Liu, et al. [37]	Shandong, China (2013–2017)	PCI/SMCI/TCI/VCI/ MCDIs /SPI/SPEI/MI	MCDIs is positively correlated with SPI-1 and MI. MCDI-1 was suitable to monitor meteorological drought and MCDI-9 was a good indicator for agricultural drought.
Wei, et al. [38]	Southwestern China (2001–2019)	PCI/SMCI/TCI/ OMDI / SPI/SPEI	There is a significant positive correlation between OMDI and grain yield as well as between OMDI and NPP in most areas of China.
Wei, et al. [39]	Northwest China (2001–2019)	PCI/SMCI/TCI/VCI/ RSDEI /SPEI	RSDEI had a strong correlation with NPP and crop yield except in some western parts of the study area.

Reviewing past studies, CI, AP, and synthetic indices based on them, have been widely used in existing drought monitoring, but there are few studies on their drought monitoring effects in southern China. In addition, the monitored results of these drought indices were usually validated by observed precipitation or statistical crop yield data. The conclusion was that the more severe the meteorological drought, the more severe the crop yield reduction (Table 1). However, contradictory phenomena are often overlooked in areas with abundant precipitation. Therefore, it is necessary to propose more effective drought monitoring methods in areas with abundant precipitation. Thus, there were three main objectives in this study: (1) to explore the applicability of the CI and AP for meteorological drought monitoring in southern China; (2) to propose a new index calculation approach, Normalized Indices (NI), for meteorological drought monitoring in southern China; and (3) to study the actual relationship between meteorological drought and crop health, such as paddy rice (*Oryza sativa* L.) and winter wheat (*Triticum aestivum* L.). The study developed a new drought index calculation method and provides a novel approach for future drought monitoring studies.

2. Study Area and Data

2.1. Study Area

The study area is located in the mid-to-lower reaches of the Yangtze River (MLRYR), extending from 24.5° N to 35.1° N and 108.4° E to 121.9° E (Figure 1). The area covers five administrative provincial units: Jiangsu, Anhui, Hubei, Jiangxi, and Hunan. While a single-cropped rice cultivation system is dominant in Jiangsu, Anhui, and Hubei Provinces, paddy rice is mainly cropped in rotation with winter wheat; a double-cropped rice cultivation system is practiced in Jiangxi and Hunan Provinces. The area has a subtropical monsoon climate with warm temperatures and abundant precipitation (Figure 2). From August to October, when crops mature, the East Asian Summer Monsoon retreats southward. Droughts and floods happen easily in this season and have caused serious economic losses and environmental damage [40–43]. In addition, the catchment area of the Yangtze River is the most concentrated area of freshwater lakes in China. Most parts of the study area are relatively flat and low-lying, including the famous Poyang and Dongting Lakes [44,45].

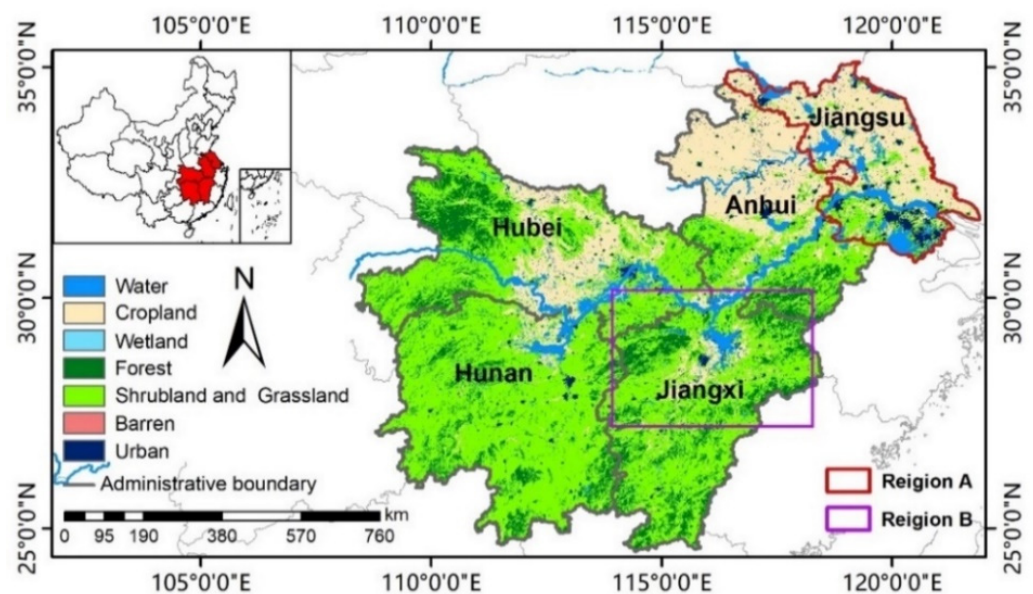


Figure 1. The study area.

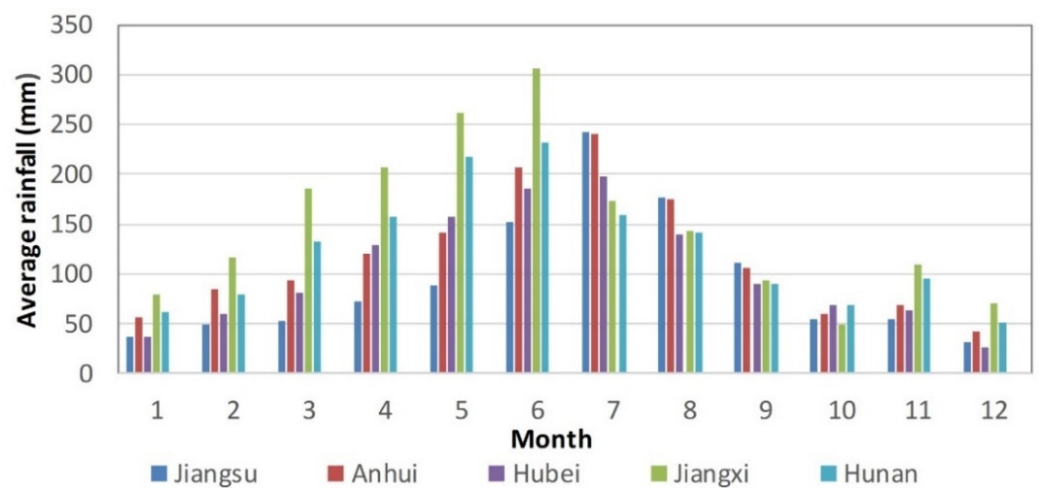


Figure 2. Average rainfall from 2003 to 2019 in study area.

2.2. Data

To achieve drought evolution process monitoring, long-term precipitation, root zone soil moisture, and vegetation data were integrated. Additionally, distribution maps of winter wheat and paddy rice were used to explore the impact of drought on crops. The crop yield data were also calculated for validation purposes. The data and related information used in this study are shown in Table 2.

Table 2. Data and related information used in the study.

Data	Source	Study Year	Temporal Resolution	Spatial Resolution
Precipitation	TRMM3B42/ TRMM3B43	2003–2019	8 days/month	0.25°
Soil Moisture	GLDAS-2.1	2003–2019	8 days/month	0.25°
Vegetation	MOD09A1/ MYD09A1	2003–2019	8 days/month	500 m
Cropland	MCD12Q1	2013	year	500 m
Wheat map	Decision Tree Classification	2011–2015	year	500 m
Rice map	PhenoRice	2011–2015	year	500 m
Growth stage	CMDSC	2011–2015	-	-
Yield	JMIC	2003–2019	year	County level

2.2.1. TRMM Data

The Tropical Rainfall Measuring Mission (TRMM), a joint project of the National Aeronautics and Space Administration (NASA) of the USA and the Japan Aerospace Exploration Agency (JAXA), was launched in November 1997 [46]. For this study, daily 3B42 precipitation data and monthly 3B43 precipitation data were used at a spatial resolution of 0.25°. The eight-day precipitation data were generated through temporal averaging of the daily 3B42 precipitation data. The precipitation data were preprocessed and downloaded on the Google Earth Engine (GEE) platform.

2.2.2. GLDAS Data

Root zone soil moisture is important and relatively stable compared with the surface soil moisture because the surface soil moisture is sensitive to other environmental variables (e.g., temperature) that drive atmospheric evaporative demand. The Global Land Data Assimilation System version 2 (GLDAS-2) has two components: one forced entirely with Princeton meteorological forcing data (GLDAS-2.0) and the other forced with a combination

of model and observation-based forcing datasets (GLDAS-2.1) [47,48]. The three-hourly GLDAS-2.1 Noah Land Surface Model L4 product at 0.25° resolution from 2003 to 2019 was used to generate the eight-day root zone soil moisture data through temporal averaging, which were preprocessed and downloaded on the GEE platform.

2.2.3. MODIS Data

The 500 m, eight-day composite surface reflectance products (MOD09A1 and MYD09A1) of the Terra and Aqua satellites from 2003 to 2019 were downloaded from NASA's Level 1 and Atmosphere Archive and Distribution System (LAADS) (26 February 2020: <https://ladsweb.modaps.eosdis.nasa.gov/search/>). With the data processing method combination of EVI2_BLUE_MY0 [49], the processing procedures mainly included image mosaicking, subsetting, spectral indices calculation, data quality labeling, cloudy pixel removal, interpolation of vegetation index images, image stacking, and Savitzky–Golay smoothing [50], all of which were implemented using Python v.3.7 programming language.

2.2.4. Land Cover Data

The distribution of winter wheat in Jiangsu Province from 2011 to 2015 came from Chen [51], and the spatial resolution had been resampled from 250 m to 500 m. The distribution of rice from 2011 to 2015 was obtained by the PhenoRice algorithm, with a resolution of 500 m [49,52]. Both maps are based on decision tree classification, combined with the phenology information of crops, with accuracies greater than 90%. The 500 m MODIS Land Cover Type products (MCD12Q1) of 2013 were downloaded from LAADS. Land_Cover_Type_1 was selected from datasets of land cover type products. The types of land cover had been merged from the original 17 categories to form 6 categories for use as a base map; the results are shown in Figure 1.

2.2.5. Other Data

Yield data of paddy rice were provided by the Jiangsu Meteorological Information Centre (JMIC) of China, including the statistical area and yield data of 72 counties in Jiangsu Province (Region A) from 2003 to 2019. The growth stage data of field observations from 2003 to 2015 were downloaded from the China Meteorological Data Service Centre (CMDSC, 25 June 2018: <http://data.cma.cn/>). The entire growing season of winter wheat was divided into two stages: Wheat Stage 1 (from sowing to the end of the regreening period—late October of the previous year to late February) and Wheat Stage 2 (from jointing period to maturity—early March to early June). The growing season of paddy rice was also divided into two stages: Rice Stage 1 (from transplanting to the end of jointing period—mid-June to late July) and Rice Stage 2 (from booting period to maturity—early August to mid-October).

3. Methodology

3.1. Calculation of the Condition Indices and Anomalies Percentage

PCI, SMCI, and VCI, calculated using TRMM, GLDAS, and MODIS data, respectively, are collectively called the Condition Indices (CI) and are computed as follows:

$$CI_i = \frac{F_i - F_{min}}{F_{max} - F_{min}} \quad (1)$$

where F_i , F_{max} , and F_{min} are the pixel values of precipitation (or root zone soil moisture or EVI2) and its maximum and minimum values, respectively. CI_i varies from 0 to 1, but a value of 0.5 is usually set as the threshold to monitor anomalous events. When CI_i equals 0.5, it is not difficult to obtain

$$F_i = Standard_{CI} = \frac{F_{max} + F_{min}}{2} \quad (2)$$

Take PCI as an example. During a meteorological drought with low precipitation, the PCI is close to or equal to 0, while during flooding conditions it is close to 1. If the PCI is less than 0.5, it means the precipitation is less than $\text{Standard}_{\text{PCI}}$.

The Precipitation Anomalies Percentage (PAP), Soil Moisture Anomalies Percentage (SMAP), and Vegetation Anomalies Percentage (VAP), collectively referred to here as the Anomalies Percentage (AP), are computed as follows:

$$AP_i = \frac{F_i - \bar{F}}{\bar{F}} \times 100\% \quad (3)$$

where F_i and \bar{F} are the pixel values of precipitation (or root zone soil moisture or EVI2), and the mean value is computed as follows:

$$\text{Standard}_{AP} = \bar{F} = \frac{F_1 + F_2 + \dots + F_n}{n} \quad (4)$$

Taking PAP as an example, in the ideal condition of a meteorological drought with low precipitation, PAP is close to or equal to -100% , while during flooding conditions the PAP is close to positive infinity. When PAP is less than 0, it means that the precipitation is less than $\text{Standard}_{\text{PAP}}$; that is, less than the average precipitation over the years.

3.2. Principle and Construction of the Normalized Indices

When using multiyear RS data to monitor drought, whether CI or AP, the purpose of the calculation is to compare with a standard value to judge the degree of drought or moisture. Therefore, this standard value needs to be typical and can represent the normal level of the pixel over a long period of time; thus, we proposed a new index calculation method named Normalized Indices (NI), the development of which is shown in Figure 3.

Name of calculation method	Formula	Standard value	Indices
Anomalies Percentage	$\frac{F_i - \bar{F}}{\bar{F}} \times 100\%$	$\bar{F} = \frac{F_1 + F_2 + \dots + F_n}{n}$	PAP/SMAP/VAP
	①	Development ①: Replace \bar{F} with \bar{F}'	
Enhanced Anomalies Percentage	$\frac{F_i - \bar{F}'}{\bar{F}'} \times 100\%$	\bar{F}'	EPAP/ESMAP/EVAP
	②	Development ②: Normalized calculation	
Normalized Indices	$\frac{F_i - \bar{F}'}{F_i + \bar{F}'}$	\bar{F}'	NPI/NSMI/NVI

Figure 3. The development of Normalized Indices. Note: \bar{F} is the mean value of precipitation (or root zone soil moisture or vegetation index) over many years. \bar{F}' is calculated by arranging the precipitation value of a single pixel over many years, from small to large, and averaging the values distributed in the middle 30–70% (40% in total).

Because the extreme values are added to the calculation of $\text{Standard}_{\text{PCI}}$ and $\text{Standard}_{\text{PAP}}$, they cannot represent well the real normal level of the pixels. Based on the AP calculation method, we use \bar{F}' instead of \bar{F} to obtain the calculation formula of Enhanced Anomalies Percentage (EAP):

$$EAP_i = \frac{F_i - \bar{F}'}{\bar{F}'} \times 100\% \quad (5)$$

\bar{F}' is calculated by arranging the precipitation value (or soil moisture/vegetation index) of a single pixel for many years, from small to large, and averaging the values distributed in the middle 30–70% (40% in total). However, when F_i exceeds twice \bar{F} (or \bar{F}'), PAP and EPAP are greater than 100%. Since there is no upper limit for PAP and EPAP under ideal conditions, the modified Normalized Indices (NI) is proposed to monitor changes in precipitation (Normalized Precipitation Index, NPI), soil moisture (Normalized Soil Moisture Index, NSMI), and crop growth status (Normalized Vegetation Index, NVI), which is defined as follows:

$$NI_i = \frac{F_i - \bar{F}'}{F_i + \bar{F}'} \quad (6)$$

NI_i varies from -1 to 1 , and the value of 0 is set as the threshold for monitoring the anomalous change:

$$Standard_{EAP} = Standard_{NI} = \bar{F}' \quad (7)$$

Take the multiyear precipitation events of typical pixels in the study area as an example (Figure 4). The area where Pixel 2 is located experienced extraordinary rainstorm events from 2003 to 2019, but Pixel 1 did not. Due to the small difference in precipitation over the years for Pixel 1, $Standard_{PCI}$, $Standard_{PAP}$, and $Standard_{NPI}$ are not very different; they are all close to the normal level. For Pixel 2, because the extreme maximum value was added to the calculation, the $Standard_{PCI}$ is much higher than the pixel values of normal years. Precipitation for all years was less than $Standard_{PCI}$, except in the year when the maximum occurred. As a result, PCI-based algorithms monitor different degrees of meteorological drought in the subsequent 16 years, which is completely inconsistent with the facts. The AP also has the same problem with CI, but the degree is relatively minor. In contrast, $Standard_{NI}$ is typical and can represent the normal level of the pixel over a long period of time.

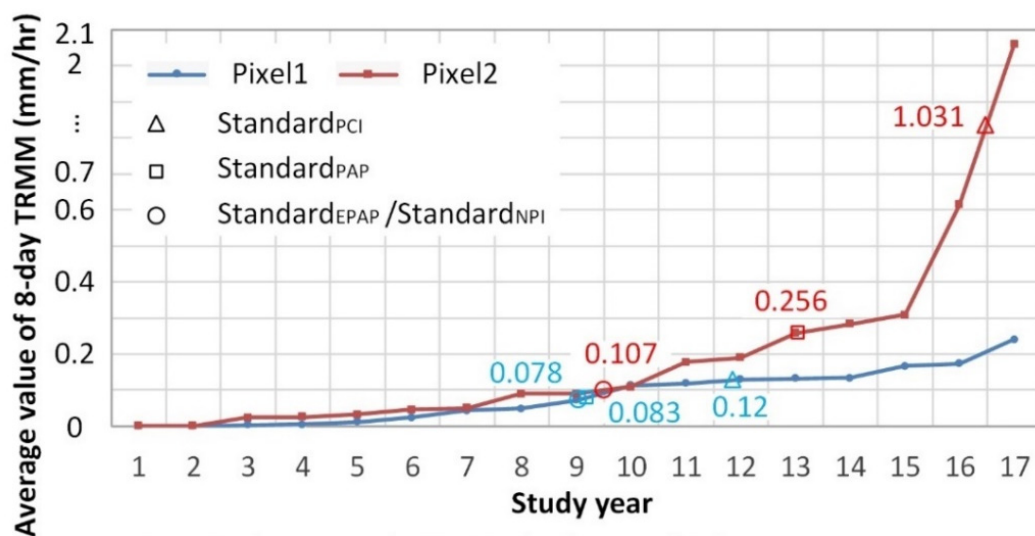


Figure 4. Time series curve of eight-day average TRMM data of typical pixels in the study area from 2003 to 2019. The row and column number of Pixel 1 is (36,50), shown in blue; Pixel 2, which encounters an abnormal rainy event with coordinates of (24,76), is given in red. Note: Study years sort by TRMM value from small to large.

3.3. Differences in Monitoring Effects of Different Indices

Take precipitation as an example. Assume that the precipitation range (true value) is between 0 and 10, where 0 means no precipitation, 10 means the maximum precipitation recorded in the history of all regions, and 5 is the normal precipitation in an ordinary semiarid and semihumid region. Among them, the omitted year (ellipsis) pixel value in the first column (Figure 5(a1,b1,c1)) is the same as in Year n . Taking Figure 5(b1) as an example, all of them are 0.25. Pixel 1 represents normal pixels that show no extreme drought or

extraordinary rainstorm event occurring, or that show places where both have occurred with similar severity in all monitoring years; Pixel 2 represents only severe drought events that occurred in a certain year; Pixel 3 represents only severe humid events that occurred (such as a sudden increase in precipitation, sudden irrigation, dry land becoming paddy field, etc.).

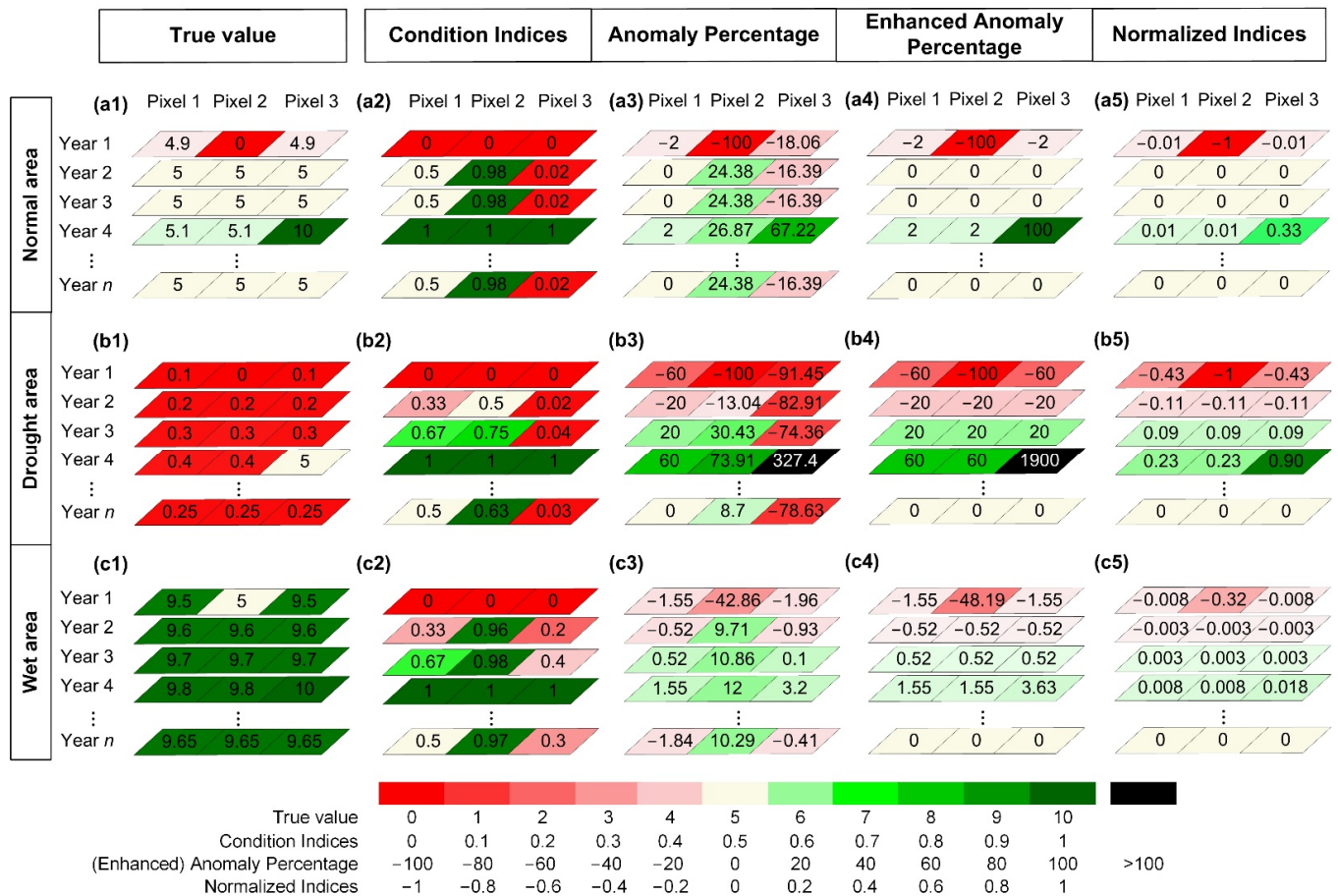


Figure 5. The simulation of different indices calculated in (a1–a5) normal regions, (b1–b5) arid regions, and (c1–c5) humid regions, using the data of various pixels for many years. Pixel 1 represents normal pixels; Pixel 2 represents pixels where only severe drought events occurred; Pixel 3 represents pixels where only severe flood events occurred.

The monitoring results of the CI (Figure 5, column 2) have two problems: (1) Once an extreme precipitation event occurs in one year, drought overestimation is likely to occur in other years. Compared with a1 and a2, Pixel 1 is a normal pixel, and the degree of drought and flood is more consistent, so the CI is relatively symmetrical; Pixel 2 only shows a severe water shortage in Year 1, which makes the CI of other nonextreme years generally larger; Pixel 3 has an extreme precipitation event in Year 4, which makes the CI of other nonextreme years generally small. In other words, for years (Year 2, Year 3, Year n, etc.) when precipitation is normal (the pixel value is 5 in a normal region), the monitoring results of CI show that Pixel 1 is consistent with the actual situation, Pixel 2 is wetter, and Pixel 3 has severe drought overestimation, compared with the actual situation (Figure 5a2). The results of b2 and c2 have the same problem as a2. This is because the Standard_{PCI} of all pixels is very different due to the extreme value being added to the calculation, as shown in Figure 5, resulting in the same true value of pixels in normal years, but the precipitation status shown by PCI is very different. (2) Due to the calculation method of the CI, there are always the values of 0 (extreme drought) and 1 (extraordinary precipitation) for each pixel, regardless of whether real extreme events occurred. It is easy to monitor extreme abnormalities (a1—Pixel 1 and a2—Pixel 1) even if the true values of pixels are similar.

NI does not have this problem (Figure 5, column 5). In regions with similar daily conditions, the same true value will have very similar monitoring results (a5/b5/c5—Years 2 and 3); for regions with different moisture conditions, the same true value will have different monitoring results, such as all the pixels with a true value of 5 in a5, b5, and c5. The true value of 5 in a1, b1, and c1 has completely different meanings: it is the normal rainfall in normal (semiarid and semihumid) regions (a1); it means high rainfall in arid regions (b1); it means low rainfall in a humid region (c1). NI can monitor the relative changes of real precipitation (or soil moisture or vegetation conditions) of pixels in different regions. It changes from -1 to 1 , which is convenient for mapping. However, the legend display of NI is not symmetrical, as shown in Table 3. The main advantages and disadvantages of CI, AP, EAP, and NI are summarized in Table 4.

Table 3. Legend meaning of Normalized Indices.

n (\times Standard)	Label	n (\times Standard)	Label	n (\times Standard)	Label
0	-1	1	0	2	0.333
0.1	-0.818	1.1	0.048	3	0.5
0.2	-0.667	1.2	0.091	4	0.6
0.3	-0.538	1.3	0.130	10	0.818
0.4	-0.429	1.4	0.167	100	0.980
0.5	-0.333	1.5	0.20	MAX	≈ 1
0.6	-0.250	1.6	0.231		
0.7	-0.176	1.7	0.259		
0.8	-0.111	1.8	0.286		
0.9	-0.053	1.9	0.310		
1	0	2	0.333		

Table 4. The advantages and disadvantages of Condition Indices, Anomalies Percentage, Enhanced Anomalies Percentage, and Normalized Indices.

Index	Advantages	Disadvantages
CI	(1) CI is accurate in places where both drought and flood have occurred with similar severity. (2) The legend display is symmetrical.	(1) Once extreme precipitation event occurs in one year, drought overestimation is likely to occur in other years and vice versa. (2) There are always the values of 0 (drought) and 1 (precipitation) for each pixel, regardless of whether the real extreme events occur.
AP	(1) AP can well present the distance between the current value and the average value.	(1) The same as point (1) of CI to a lesser degree. (2) There is no upper limit under ideal conditions.
EAP	(1) EAP can monitor the relative changes of real situation of pixels in both arid and humid regions.	(1) There is no upper limit under ideal conditions.
NI	(1) NI does not have the limitations of above indices, and can monitor the relative changes of real precipitation (or soil moisture or vegetation conditions) of pixels in both arid and humid regions.	(1) The legend display is not symmetrical.

The monitoring results of the AP (Figure 5, column 3) have the following problems: (1) The first problem of CI, but the degree is relatively minor. When extreme events occur in certain years of the pixel, for other years with normal pixel values (Year 2, Year 3, Year n , etc.), the monitoring results using AP will be wetter (a3,b3,c3—Pixel 2) or drier

(a3,b3,c3—Pixel 3) than the actual situation. (2) When the pixel value exceeds twice \bar{F} (or \bar{F}'), the AP will be greater than 100%. The monitoring results of the EAP (Figure 5, column 4) do not have the first problem of the AP, but the second problem persists.

3.4. Validation of Study Results

The *Yearbook of Meteorological Disasters in China* and crop yield data from 2003 to 2019 were used to validate the study results. The drought and flood events recorded in the disaster yearbook are a summary of the meteorological observation data of China's meteorological departments at all levels and of the on-site monitoring results of meteorological stations. The main resource for drought and flood disaster analysis is precipitation data from field observations. In addition, when a severe drought is encountered, there will be records related to the state of soil moisture and crops, facilitating a comprehensive validation of remote sensing monitoring results. We also conducted a field survey in Jiangxi Province (Region B) in 2019 as a supplement, to validate the RS monitoring results.

Meteorological disasters, insects, diseases, and nutrients can all affect crop health and yield variation, but the meteorological factor is usually the main factor in crop monitoring of a large region. In this study, we used the changes in vegetation index to monitor the health of crops. The correlation between NVI and crop yield was used to validate the vegetation index monitoring results. Except for the Yield Anomalies Percentage (YAP) and Normalized Yield Index (NYI), the Standardized Variable of Yield (SVY) of each county [35] was also used to monitor the variation of crop yield, which is calculated as follows:

$$SVY_i = \frac{Y_i - \bar{Y}}{\sigma} \times 100\% \quad (8)$$

where Y_i is the crop yield in i year of one county, \bar{Y} is the average, and σ is the standard deviation of crop yield from 2003 to 2019.

4. Results

4.1. Application and Results Validation of Different Indices

4.1.1. Temporal Differences in PCI, PAP, EPAP, and NPI

Region A experienced continuous rainy weather from 6 August to 18 September 2014. The province's average precipitation was 60% higher than in the same period in normal years, which has been rare in recent years. This included a number of heavy rainstorms, sometimes accompanied by typhoons, which caused water to accumulate in farmland and crops to fail. From mid-June to late July 2014, there was a severe precipitation reduction, and the precipitation in December was also much lower than in previous years (as recorded in the *Yearbook of Meteorological Disasters in China*).

Compared with the actual results, PCI was significantly lower than the actual precipitation, so the rainy weather from 6 August to 18 September could not be monitored (Figure 6). This was because, compared with normal pixels that had no extreme events, pixels with extraordinary rainstorm events occurred and would have larger values of $\text{Standard}_{\text{PCI}}$, as shown in Figure 6—Pixel 2, resulting in a lower PCI value for normal years (Figure 5(a2,b2,c2)—Pixel 3). The results of PCI would suggest more severe drought events than the actual situation. Compared with PCI, the trend changes in precipitation monitored by PAP were more realistic. EPAP tended to have a value greater than the upper limit of the map display (far greater than 100%), which was not conducive to statistics and display. The NPI could monitor well the abnormal events of precipitation in the long-term series. The monitoring of the start and end time of the abnormal event was also more accurate and in line with the actual situation.

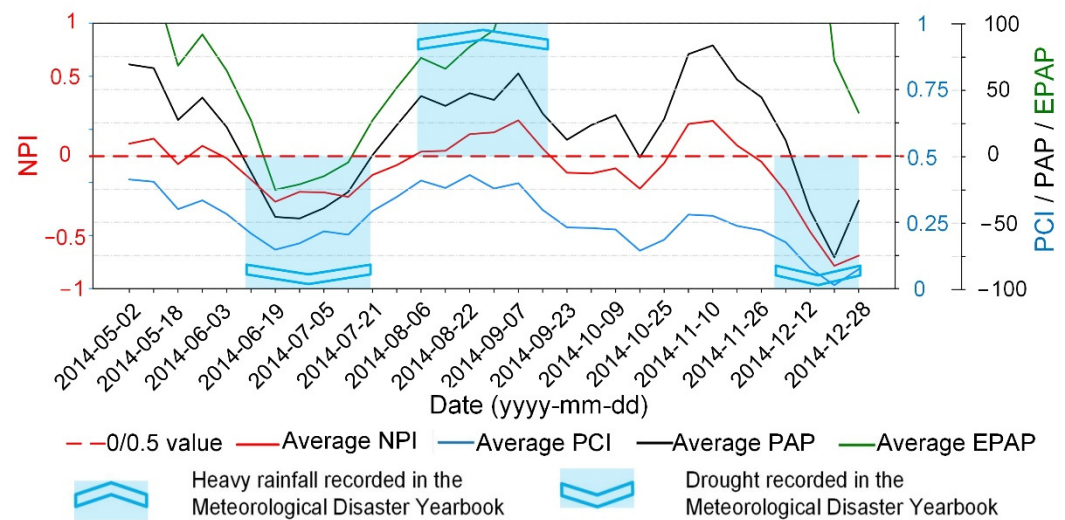


Figure 6. Average crop pixel values of PCI, PAP, EPAP, and NPI in Region A from May 2014 to December 2014, while PCI, PAP, EPAP, and NPI were updated every eight days and are marked in different colors; 0.5 is the threshold of PCI, whereas the other indices use 0.

4.1.2. Spatial Differences in Normalized Indices and Condition Indices

Regional changes and intensity changes in precipitation in the entire study area monitored by NPI from July to October were highly consistent with the drought and heavy rain events recorded in the yearbook. The changes in soil moisture monitored by NSMI were also in good agreement with changes in precipitation (NPI) (Figure 7a). The following *Yearbook* records are introduced in chronological order (months): (1) There were torrential rains and floods in the study area in July 2014, while a moderate to severe meteorological drought occurred in north-central Jiangsu, northwest Anhui, and central Hubei in the same month. (2) From 7 to 31 August, there were continuous low temperatures and rainy weather in the entire study area. The temperature in most areas was 2–3 °C lower than normal, and the sunshine hours were 60–80 h fewer than normal. Among them, the sunshine hours in Jiangsu Province were the lowest since 1961. The continuous low temperature and inadequate illumination in August caused damage to vegetation growth and decreased NVI (Figure 7a). (3) Jiangsu Province experienced continuous rainy weather from 1 to 18 September; Anhui Province's average precipitation was 32 days from 1 August to 30 September, the most in the same period since 1961; there were continuous rainy days in most parts of Hubei Province from 8 to 19 September. (4) However, drought occurred in central and southern Jiangxi from mid-September to early November and obvious meteorological droughts occurred in southern and eastern Hunan from mid-September to late October. From 16 to 21 October, there was continuous rain in western Hubei; from 27 to 30 October, there was continuous heavy rainfall in the MLRYR. Heavy to extreme rain occurred in some regions, which adversely affected crop growth (2014 *Yearbook of Meteorological Disasters in China*).

Compared with the meteorological observation results, the precipitation events monitored by PCI from July to October 2014 were generally small in scope and low in intensity, as shown in the purple circles of Figure 7. The results of soil moisture distribution monitored by SMCI were quite different from the PCI results. For example, except for Hubei Province, August showed continuous rainy weather with little sunshine; the PCI monitoring result was that the precipitation was relatively low, while the soil moisture monitored by the SMCI was obviously humid. This is mainly because the precipitation event in August had a long duration and wide range, but the overall intensity was not large. The total monthly rainfall was not high in the same month of all years, so the PCI monitoring result was drought (as shown in Figure 7b), which did not match the actual situation. For regions that suffered heavy rainfall events, the monitoring results of the Condition Indices would

reflect severe drought overestimation, in which the error of precipitation (PCI) would be greater than that of soil moisture and vegetation (SMCI and VCI).

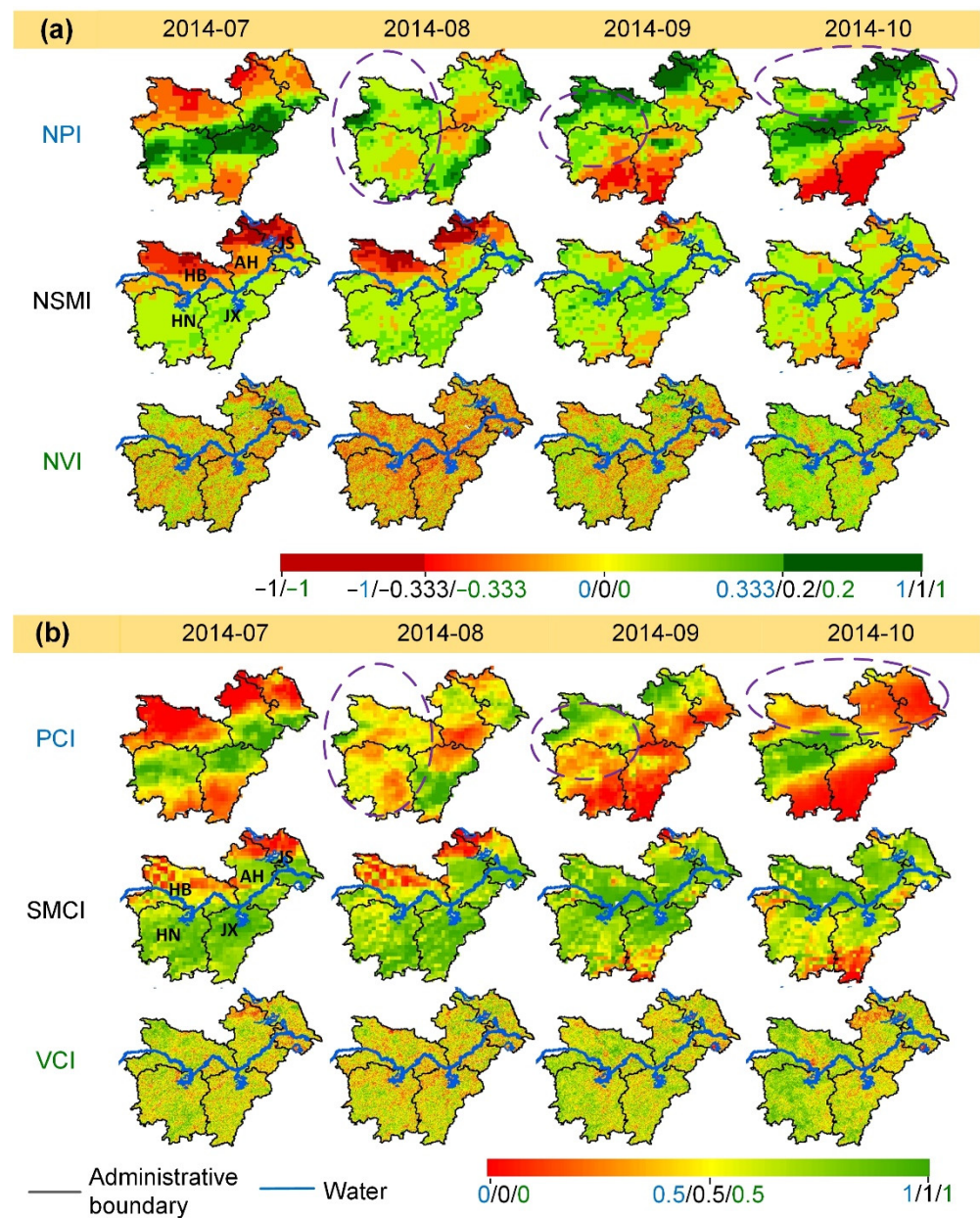


Figure 7. Spatial evolution of NPI/NSMI/NVI (a) and PCI/SMCI/VCI (b) in Jiangsu, Anhui, Hubei, Jiangxi, and Hunan Provinces, China. The results are organized on a timeline from July 2014 to October 2014 (the main growth season of rice). All indices were updated monthly.

4.2. Multiyear Drought Monitoring Based on Normalized Indices

4.2.1. Temporal Evolution of NPI, NSMI, and NVI

The PCI from 2011 to 2015 was below 0.5, indicating a four-year meteorological drought event that was obviously inconsistent with the facts; it did not match the excessive precipitation events recorded in the *Yearbook* (Figure 8a). The NPI could better monitor the drought and precipitation events recorded in the *Yearbook* than PCI (Figure 8b). The difference between VCI and NVI was smaller than that between PCI and VCI because the weather-related part of EVI2 affected by weather changes (precipitation, drought, high temperature, etc.) was relatively small [16], leading to more accurate results for VCI. How-

ever, the occasional excessive rainfall increases the value of Standard_{PCI}, making the PCI of normal years relatively small and causing the overestimation of meteorological drought.

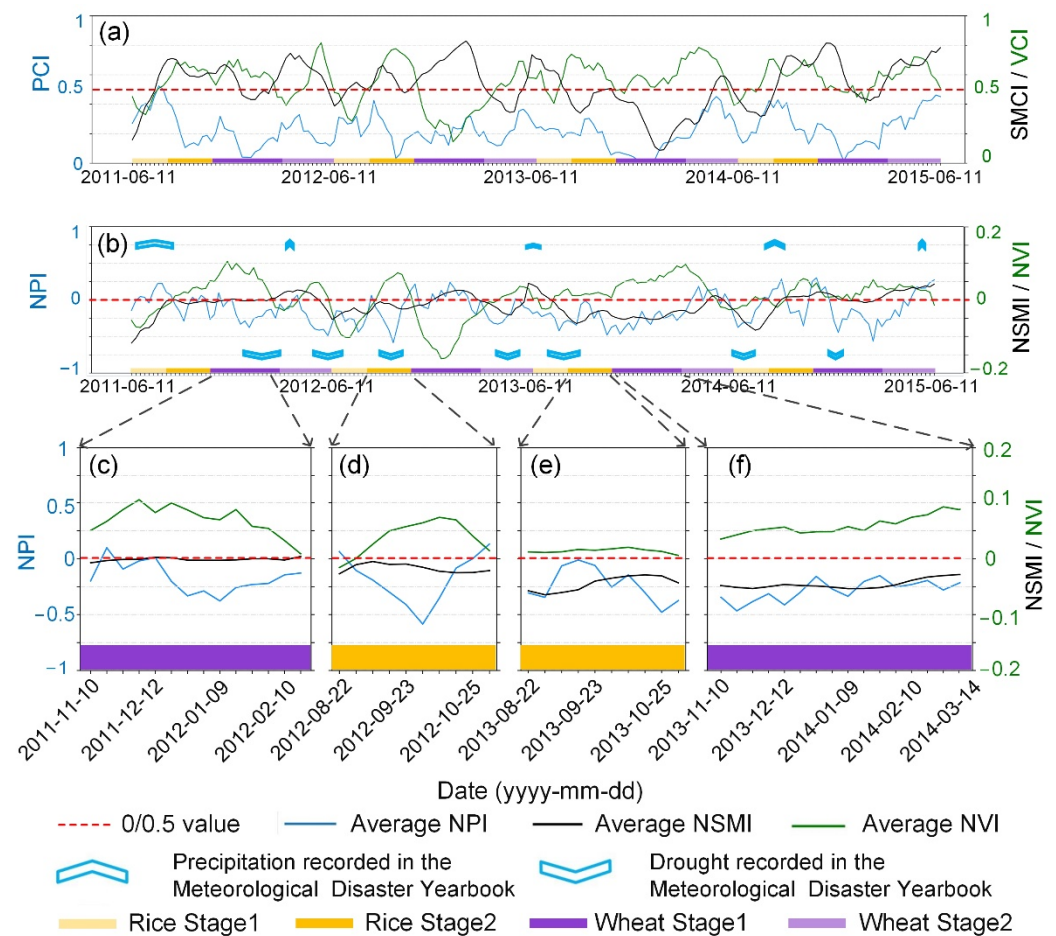


Figure 8. Average values of wheat and rice pixels of PCI/SMCI/VCI (a) and NPI/NSMI/NVI (b). (c–f) NI temporal evolution of four typical meteorological drought events in detail. The values of 0.5 and 0 are the threshold of CI and NI, respectively; meteorological drought is indicated when PCI is less than 0.5 or NPI is less than 0. Wheat Stage 1 means the sowing to regreening period of wheat; Wheat Stage 2 means the jointing to maturity; Rice Stage 1 means the transplanting to the jointing period of rice; Rice Stage 2 means the booting to maturity (see Section 2.2.5). All indices were updated every eight days and are marked in different colors.

It is especially worth noting that when the NPI was less than 0, the NVI (Figure 8b–f) was greater than 0; in other words, when meteorological drought (precipitation lower than the normal level) occurred, the crops grow better in Rice Stage 2 and wheat growing seasons in the MLRYR. This is because, in arid regions that rely on precipitation for irrigation, water is the main factor affecting crop health. However, in the MLRYR, which has abundant precipitation and numerous rivers and lakes, the continuous rainy weather is usually accompanied by reduced illumination and lower temperatures, which are not conducive to crop growth. In contrast, the meteorological drought means adequate illumination in the MLRYR, so crops grow better. However, during the wheat sowing period or rice transplanting period, severe meteorological drought will affect the growth and survival of seedlings, which causes serious damage to crops.

4.2.2. Spatial Evolution of Drought in 2019

In the postmonsoon (August–October) season of 2019 [53], there was great public concern about the severe drought event in the MLRYR, so we carried out a week-long field

survey in Region B of Jiangxi Province in late October 2019. We visited the Agricultural Meteorological Center, surveyed a total of 180 rice samples (evenly distributed in the main rice-growing areas), and interviewed 12 rice growers to understand the evolution of drought (Figure 9).

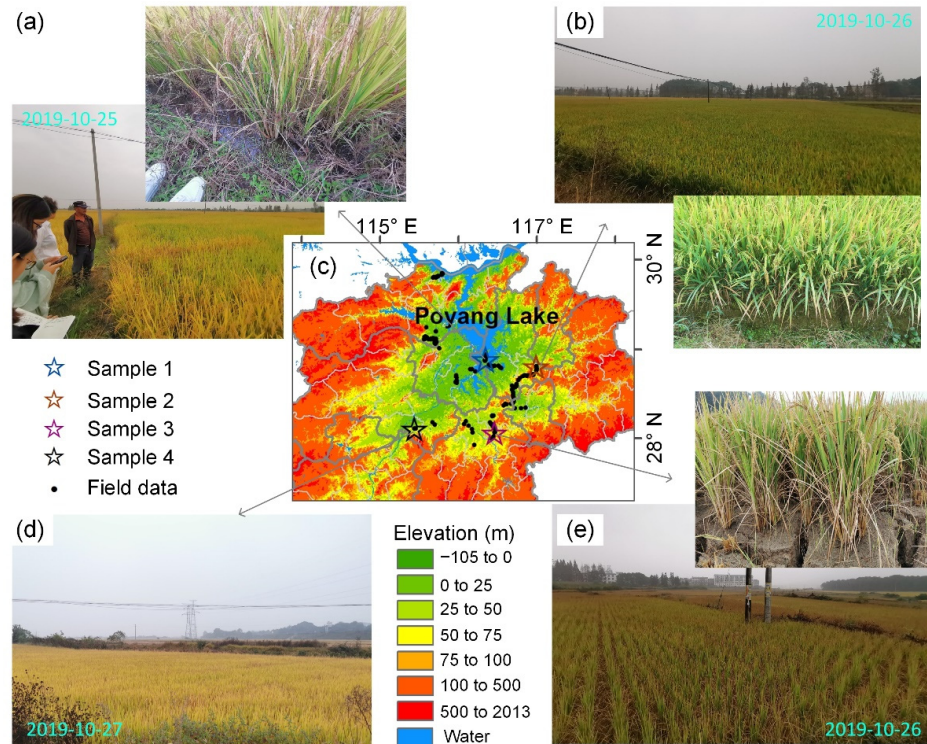


Figure 9. Field survey and ground geotagged photos of paddy rice with different health conditions in Region B in late October 2019. (c) Topography of Region B and the distribution of field survey points; (a,b,d) rice paddies with irrigation; (e) rice paddies without irrigation.

The survey results showed that Region B had abundant precipitation before August, and some regions had more than 40 consecutive days of precipitation before 14 July. Starting in late July, most areas of Region B had more than 100 consecutive days without precipitation. The growth conditions of rice were roughly divided into three types: (1) In most areas, due to the large water storage capacity of the reservoir and the good irrigation system, the soil moisture was normal or slightly lower than in previous years. The growth of rice was not significantly affected (Figure 9b,d) and the estimated yield had not changed obviously from previous years. (2) In the area close to Poyang Lake, water could be seen in the fields (Figure 9a). Due to the abundant sunshine from August to October, a slight increase in yield was expected. (3) In the small area with higher altitudes or poorer irrigation conditions, the soil moisture was obviously lower, reducing the yield by about 50% (Figure 9e) or even resulting in no harvest.

The NPI-based precipitation monitoring results showed severe meteorological drought (Figure 10). The soil moisture of most pixels in the entire study area was lower than that of the same period by about 20%. Since the soil moisture in the MLRYR was high in normal years, the reduction in soil moisture in most parts of the study area did not cause serious damage to vegetation growth. The NVI of the entire study area increased from -0.015 in July to 0.012 in October month by month, indicating that the vegetation growth showed a tendency to improve.

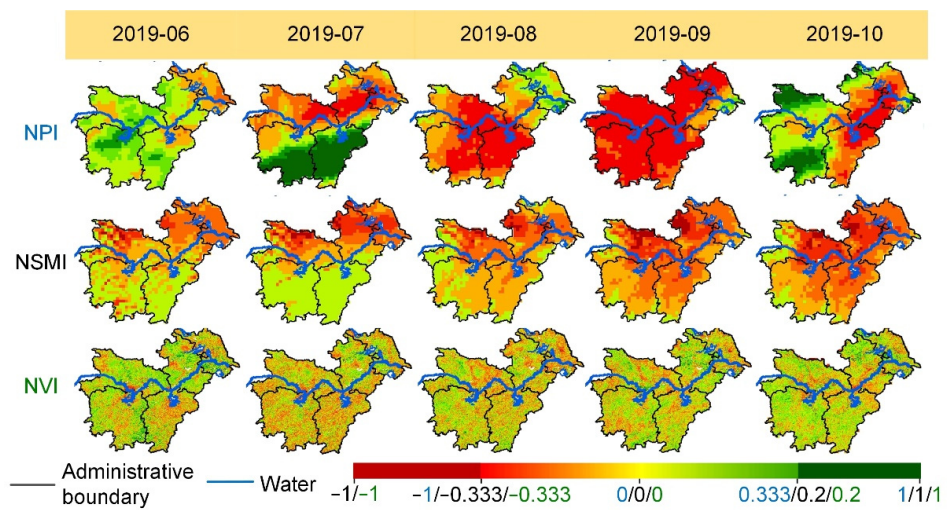


Figure 10. Spatial evolution of NPI, NSMI, and NVI in study area from June to October 2019 (growth season of rice). All indices were updated monthly.

We used changes in the vegetation index to monitor the crop health and the correlation between NVI and crop yield to validate the vegetation index monitoring results. The NPI and NVI of the main growing season of rice in Region A were averaged, and the results (Figure 11a,b) showed that the meteorological drought in the east was more serious but that the EVI2 had increased compared with previous years because there were more lakes in the western part of Region A. Compared with the average value of the entire rice growing season, the NVI of the harvest period was more consistent with the spatial variation of rice yields (Figure 11c,f). The effect of increasing production in the west was more obvious than in the east and, compared with YAP (Figure 11d) and SVY (Figure 11e), the spatial variation of NYI (Figure 11f) was more consistent with NVI. Both the vegetation index and the rice yield were negatively correlated with precipitation (Figure 12). With the decrease in precipitation, the vegetation index of 78.8% of pixels increased, while the yield of 97.1% of pixels increased.

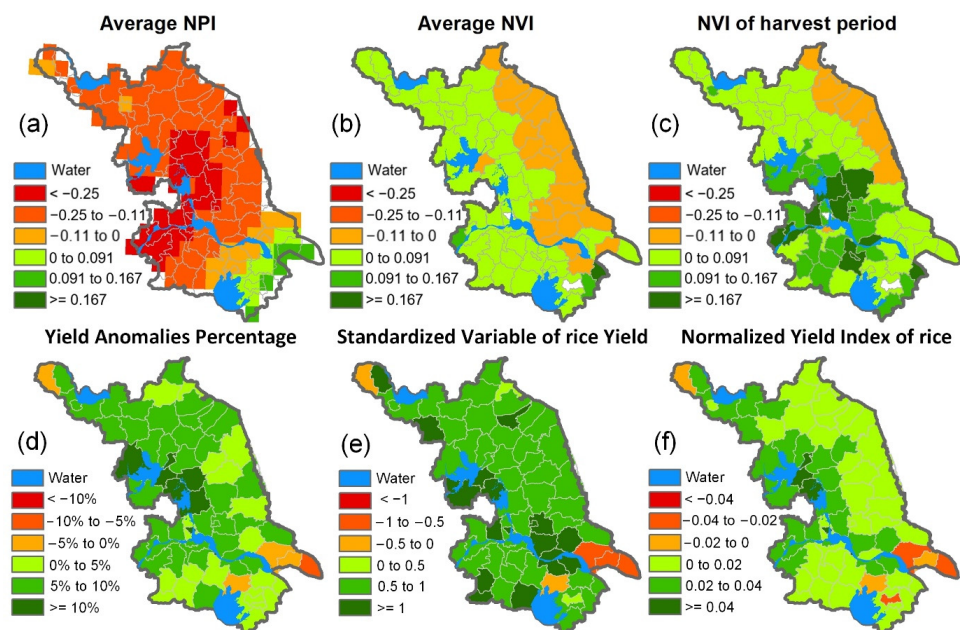


Figure 11. Spatial evolution of NPI, NVI, and rice yield change of Region A in growth season of rice in 2019.

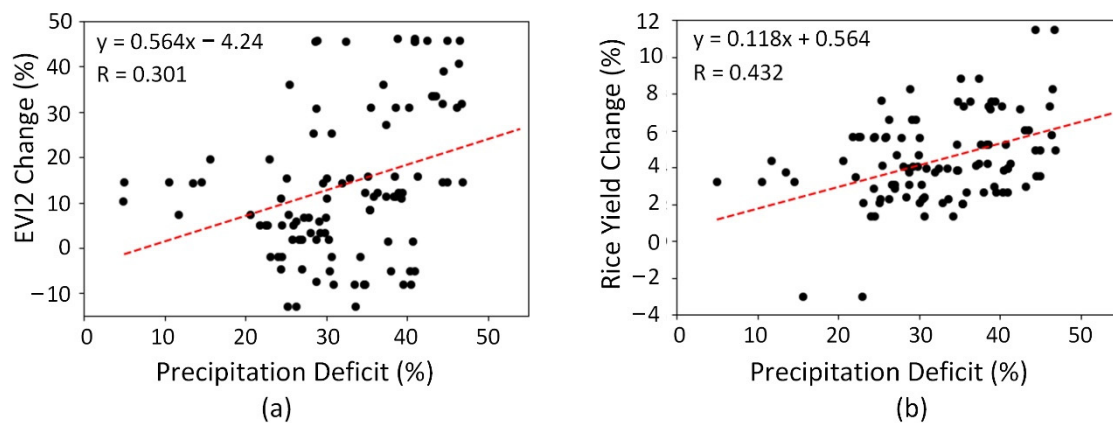


Figure 12. Scatter plot and correlation analysis between precipitation deficit, vegetation index (a), and rice yield (b) of region A in 2019.

5. Discussion

Most of our understanding of drought is based on remote sensing data, using calculated RS drought indices to monitor the conditions of precipitation, soil moisture, temperature, and vegetation. Each factor was assigned different weights based on empirical analysis, principal component analysis (PCA), kernel entropy component analysis (KECA), spatial principal component analysis (SPCA), and other methods [23,35,54,55]. New composite drought indices were then formed and used to monitor meteorological drought, agricultural drought, or hydrological drought in different regions. When using RS data for many years in drought monitoring, the purpose of the calculation is to compare the current state with a standard value, judging the drought or moisture degree in the region at a certain time. Due to the calculation principle of existing Condition Indices and Anomalies Percentage, drought overestimation occurs easily, especially in regions with abundant precipitation. However, the $Standard_{NI}$ can better represent the normal level of a region, which makes the results of precipitation, soil moisture, and vegetation changes monitored by Normalized Indices more consistent with the actual situation. Based on Normalized Indices, we realized the accurate monitoring of meteorological drought events in the study area over many years.

In addition, we studied the well-known meteorological drought event that occurred in the MLRYR from August to October 2019 and found that it had a much less severe impact on vegetation than expected. Meteorological or climatological drought is defined simply in terms of the magnitude and duration of a precipitation shortfall (16 August 2020: <https://www.ametsoc.org/index.cfm/ams/about-ams/ams-statements/statements-of-the-ams-in-force/drought/>). When a severe meteorological drought event occurs, people generally associate it with damaged crops and reduced yields. This phenomenon is evident in arid regions that rely solely on precipitation irrigation, which is also the focus of most studies. However, the fact that meteorological drought induces an increase in the vegetation index and crop yield is readily overlooked due to the lack of systematic studies. Our investigations have found that in southern China the water demand of crops can be satisfied by irrigation when meteorological drought occurs. The irrigation sources include lakes, reservoirs, pond water storage, and underground pumping. At the same time, a reduction in rainfall means an increase in illumination and adequate heat resources, so crops grow better. Anderson et al. [56] suggested that a finer crop model was needed that could consider moisture and temperature extremes during critical phenological stages of crop growth. We should also give more attention to the illumination. In addition, in accordance with the definition of meteorological drought as only a shortage of rainfall, it is not recommended to add on other factors such as soil moisture or vegetation; this would cause adverse effects because precipitation is not simply positively correlated with the vegetation index.

Agricultural drought links meteorological drought characteristics to agricultural impacts, associating precipitation shortages most immediately with higher evapotranspiration levels and soil moisture deficits. Our results prove that severe precipitation deficiency and meteorological drought do not necessarily lead to agricultural drought. Even when precipitation is the main water input for crops, in some regions a statistically weak relationship between precipitation and yield loss may be seen [36,57], while the timing of the precipitation is also an important factor. Therefore, it is not sufficient to use only measured precipitation to assist in the construction of agricultural drought monitoring models (such as determining the weight of each component) or for validating the monitoring results. Our results can provide some new ideas for the construction of agricultural insurance models.

Despite the good performance at capturing drought impacts, some key limitations exist when using Normalized Indices, as seen in this study.

The first limitation was introduced by the computation method. When calculating Condition Indices or Anomalies Percentage using soil moisture or vegetation index data over many years, the types of land cover are not distinguished, which is also one of the sources of error. For example, there was one area where a certain pixel had been represented as dry land for many years and only one year where it was used as a paddy field. When calculating CI or AP, if this single “paddy field” year was not removed using land cover data, other years would have appeared as having low soil moisture and severe drought, which was inconsistent with the real situation (Pixel 3 of Figure 5(a1,a2)). Land cover changes, such as crops to trees or farmland to ponds, will also increase the error in drought monitoring. Using Normalized Indices can avoid calculation errors, but the land use inconsistency of time series can also cause errors in judgment. Therefore, the use of multiyear land cover data to filter the time series in index calculations can improve the accuracy of disaster identification. Another limitation is the data requirement. The spatial resolution of the data used in this study was too low, especially for soil moisture. It is necessary to use the same resolution for soil moisture data as for the vegetation index. Soil moisture is a factor that directly impacts vegetation health, and the response of different vegetation changes in soil moisture varies. Adding high-spatiotemporal-resolution soil moisture data will be the basis for the high-precision monitoring of agricultural drought in the future.

6. Conclusions

According to the calculation principle of commonly used RS drought indices, and for achieving more accurate drought monitoring, we proposed a new index calculation method, referred to as Normalized Indices or NI. TRMM precipitation, GLDAS soil moisture, and MODIS reflection datasets were used to calculate drought indices. The disaster events recorded in the *Yearbook of Meteorological Disasters in China*, field survey data, and statistical crop yield data were used to validate the monitoring results of paddy rice and winter wheat. Through the simulation of different types of moisture conditions and multiyear drought monitoring of the study area, the monitoring results showed:

- NI can monitor well the relative changes in real precipitation/soil moisture/vegetation conditions, in both arid and humid regions, while meteorological drought is easily overestimated with CI in areas with abundant precipitation;
- The error of precipitation (PCI) is greater than that of soil moisture and vegetation (SMCI and VCI), the same as AP;
- The well-known drought event that occurred in the MLRYR from August to October 2019 had a much less severe impact on vegetation than expected. In contrast, the precipitation deficiency induced an increase in sunshine and adequate heat resources, which improved crop growth in most areas.

This study shows some restrictions and shortcomings of recognized CI and AP, and it proposes a new index calculation method of NI to better monitor meteorological drought in the MLRYR of China, providing a new method for future drought monitoring studies.

Author Contributions: Conceptualization and resources, J.H.; methodology and software, L.L.; validation, Y.C. (Yan Chen) and P.W.; formal analysis, Y.C. (Yuanyuan Chen); investigation, W.L. and D.D.; data curation, Y.C. (Yan Chen); writing—original draft preparation, L.L.; writing—review and editing, J.C.; visualization, Q.S.; supervision, R.H.; project administration, J.H.; funding acquisition, J.H. All authors have read and agreed to the published version of the manuscript.

Funding: This research was funded by “National Key R&D Program of China”, grant number 2017YFD0300402-3 and Erasmus+ Programme of the European Union (Grant NO. 598838-EPP-1-2018-EL-EPPKA2-CBHE-JP).

Institutional Review Board Statement: Not applicable.

Informed Consent Statement: Not applicable.

Acknowledgments: We would like to thank the Jiangsu Meteorological Bureau of China for the data support. The editors’ and anonymous reviewers’ valuable comments and advice that were significant for improving this manuscript are also much appreciated.

Conflicts of Interest: The authors declare no conflict of interest.

Abbreviations

AMSR-E	Advanced Microwave Scanning Radiometer for Earth Observing System
AP	Anomalies Percentage
AVHRR	Advanced Very High Resolution Radiometer
CI	Condition Indices
CMDSC	China Meteorological Data Service Centre
EAP	Enhanced Anomalies Percentage
EPAP	Enhanced Precipitation Anomalies Percentage
ESMAP	Enhanced Soil Moisture Anomalies Percentage
EVAP	Enhanced Vegetation Anomalies Percentage
EVI2	2-band Enhanced Vegetation Index
GEE	Google Earth Engine
GLDAS	Global Land Data Assimilation System
JAXA	Japan Aerospace Exploration Agency
JMIC	Jiangsu Meteorological Information Centre
KECA	Kernel Entropy Component Analysis
LAADS	NASA’s Level 1 and Atmosphere Archive and Distribution System
MCDIs	Composite Drought Indices based on multivariable linear regression
MI	Moisture Index
MIDI	Microwave Integrated Drought Index
MLRYR	Mid-to-Lower Reaches of the Yangtze River
MODIS	Moderate-resolution Imaging Spectroradiometer
NASA	National Aeronautics and Space Administration
NDDI	Normalized Difference Drought Index
NDVI	Normalized Difference Vegetation Index
NDWI	Normalized Difference Water Index
NI	Normalized Indices
NMDI	Normalized Multiband Drought Index
NPI	Normalized Precipitation Index
NPP	Net Primary Productivity
NSMI	Normalized Soil Moisture Index
NVI	Normalized Vegetation Index
NYI	Normalized Yield Index
OMDI	Optimized Meteorological Drought Index
PADI	Process-based Accumulated Drought Index
PAP	Precipitation Anomalies Percentage
PCA	Principal Component Analysis
PCI	Precipitation Condition Index
PDSI	Palmer Drought Severity Index

PR	Precipitation Radar
PSMCI	TRMM Precipitation and Soil Moisture Condition Index
PTCI	TRMM Precipitation and Temperature Condition Index
RS	Remote Sensing
RSDEI	Remote Sensing Drought Evaluation Index
SDCI	Scaled Drought Condition Index
SDI	Synthesized Drought Index
SMAP	Soil Moisture Anomalies Percentage
SMCI	Soil Moisture Condition Index
SMTCI	Soil Moisture and Temperature Condition Index
SPCA	Spatial Principal Component Analysis
SPEI	Standardized Precipitation Evapotranspiration Index
SPI	standardized precipitation index
SVY	Standardized Variable of crop Yield
TCI	Temperature Condition Index
TMI	TRMM Microwave Imager
TRMM	Tropical Rainfall Measuring Mission
VAP	Vegetation Anomalies Percentage
VCI	Vegetation Condition Index
VIRS	Visible and Infrared Scanner
YAP	Yield Anomalies Percentage

References

- Halwatura, D.; McIntyre, N.; Lechner, A.; Arnold, S. Capability of meteorological drought indices for detecting soil moisture droughts. *J. Hydrol. Reg. Stud.* **2017**, *12*, 396–412. [\[CrossRef\]](#)
- Lai, C.; Zhong, R.; Wang, Z.; Wu, X.; Chen, X.; Wang, P.; Lian, Y. Monitoring hydrological drought using long-term satellite-based precipitation data. *Sci. Total. Environ.* **2019**, *649*, 1198–1208. [\[CrossRef\]](#)
- Dou, Y.; Huang, R.; Mansaray, L.R.; Huang, J. Mapping high temperature damaged area of paddy rice along the Yangtze River using Moderate Resolution Imaging Spectroradiometer data. *Int. J. Remote Sens.* **2019**, *41*, 471–486. [\[CrossRef\]](#)
- Sun, S.; Li, Q.; Li, J.; Wang, G.; Zhou, S.; Chai, R.; Hua, W.; Deng, P.; Wang, J.; Lou, W. Revisiting the evolution of the 2009–2011 meteorological drought over Southwest China. *J. Hydrol.* **2019**, *568*, 385–402. [\[CrossRef\]](#)
- Javed, T.; Li, Y.; Rashid, S.; Li, F.; Hu, Q.; Feng, H.; Chen, X.; Ahmad, S.; Liu, F.; Pulatov, B. Performance and relationship of four different agricultural drought indices for drought monitoring in China’s mainland using remote sensing data. *Sci. Total. Environ.* **2021**, *759*, 143530. [\[CrossRef\]](#)
- Agutu, N.; Awange, J.; Zerihun, A.; Ndehedehe, C.E.; Kuhn, M.; Fukuda, Y. Assessing multi-satellite remote sensing, reanalysis, and land surface models’ products in characterizing agricultural drought in East Africa. *Remote Sens. Environ.* **2017**, *194*, 287–302. [\[CrossRef\]](#)
- Yao, N.; Li, Y.; Sun, C. Effects of changing climate on reference crop evapotranspiration over 1961–2013 in Xinjiang, China. *Theor. Appl. Clim.* **2018**, *131*, 349–362. [\[CrossRef\]](#)
- Zhao, M.; Huang, S.; Huang, Q.; Wang, H.; Leng, G.; Xie, Y. Assessing socio-economic drought evolution characteristics and their possible meteorological driving force. *Geomat. Nat. Hazards Risk* **2019**, *10*, 1084–1101. [\[CrossRef\]](#)
- Tucker, C.J.; Townshend, J.R.; Goff, T.E. African Land-Cover Classification Using Satellite Data. *Science* **1985**, *227*, 369–375. [\[CrossRef\]](#)
- Hielkema, J.U.; Prince, S.D.; Astle, W.L. Rainfall and vegetation monitoring in the Savanna Zone of the Democratic Republic of Sudan using the NOAA Advanced Very High Resolution Radiometer. *Int. J. Remote Sens.* **1986**, *7*, 1499–1513. [\[CrossRef\]](#)
- Malingreau, J.-P. Global vegetation dynamics: satellite observations over Asia. *Int. J. Remote Sens.* **1986**, *7*, 1121–1146. [\[CrossRef\]](#)
- Justice, C.O.; Townshend, J.R.G.; Holben, B.N.; Tucker, C.J. Analysis of the phenology of global vegetation using meteorological satellite data. *Int. J. Remote Sens.* **1985**, *6*, 1271–1318. [\[CrossRef\]](#)
- Kogan, F.N. Remote sensing of weather impacts on vegetation in non-homogeneous areas. *Int. J. Remote Sens.* **1990**, *11*, 1405–1419. [\[CrossRef\]](#)
- Liu, W.T.; Kogan, F.N. Monitoring regional drought using the Vegetation Condition Index. *Int. J. Remote Sens.* **1996**, *17*, 2761–2782. [\[CrossRef\]](#)
- Kogan, F.N. Global Drought Watch from Space. *Bull. Am. Meteorol. Soc.* **1997**, *78*, 621–636. [\[CrossRef\]](#)
- Kogan, F.N. Droughts of the Late 1980s in the United States as Derived from NOAA Polar-Orbiting Satellite Data. *Bull. Am. Meteorol. Soc.* **1995**, *76*, 655–668. [\[CrossRef\]](#)
- Kogan, F. Application of vegetation index and brightness temperature for drought detection. *Adv. Space Res.* **1995**, *15*, 91–100. [\[CrossRef\]](#)
- Rhee, J.; Im, J.; Carbone, G. Monitoring agricultural drought for arid and humid regions using multi-sensor remote sensing data. *Remote Sens. Environ.* **2010**, *114*, 2875–2887. [\[CrossRef\]](#)

19. Zhang, A.; Jia, G. Monitoring meteorological drought in semiarid regions using multi-sensor microwave remote sensing data. *Remote Sens. Environ.* **2013**, *134*, 12–23. [[CrossRef](#)]
20. Ghaleb, F.; Mario, M.; Sandra, A.N. Regional Landsat-Based Drought Monitoring from 1982 to 2014. *Climate* **2015**, *3*, 563–577. [[CrossRef](#)]
21. Jiao, W.; Wang, L.; Novick, K.A.; Chang, Q. A new station-enabled multi-sensor integrated index for drought monitoring. *J. Hydrol.* **2019**, *574*, 169–180. [[CrossRef](#)]
22. Jiao, W.; Tian, C.; Chang, Q.; Novick, K.A.; Wang, L. A new multi-sensor integrated index for drought monitoring. *Agric. For. Meteorol.* **2019**, *268*, 74–85. [[CrossRef](#)]
23. Hao, Z.; Singh, V.P. Drought characterization from a multivariate perspective: A review. *J. Hydrol.* **2015**, *527*, 668–678. [[CrossRef](#)]
24. Najem, S.; Al Bitar, A.; Faour, G.; Jarlan, L.; Mhawej, M.; Fadel, A.; Zribi, M. Drought Assessment using Micro-Wave Timeseries of Precipitation and Soil Moisture Over the Mena Region. In Proceedings of the 2020 Mediterranean and Middle-East Geoscience and Remote Sensing Symposium (M2GARSS), Tunis, Tunisia, 9–11 March 2020; pp. 289–292. [[CrossRef](#)]
25. Wei, W.; Pang, S.; Wang, X.; Zhou, L.; Xie, B.; Zhou, J.; Li, C. Temperature Vegetation Precipitation Dryness Index (TVPDI)-based dryness-wetness monitoring in China. *Remote Sens. Environ.* **2020**, *248*, 111957. [[CrossRef](#)]
26. Zhang, Q.; Yu, H.; Sun, P.; Singh, V.P.; Shi, P. Multisource data based agricultural drought monitoring and agricultural loss in China. *Glob. Planet. Chang.* **2019**, *172*, 298–306. [[CrossRef](#)]
27. Qian, W.; Ai, Y.; Leung, J.C.-H.; Zhang, B. Anomaly-based synoptic analysis and model product application for 2020 summer southern China rainfall events. *Atmos. Res.* **2021**, *258*, 105631. [[CrossRef](#)]
28. Li, X.; Huang, W.-R. How long should the pre-existing climatic water balance be considered when capturing short-term wetness and dryness over China by using SPEI? *Sci. Total. Environ.* **2021**, *786*, 147575. [[CrossRef](#)]
29. Sgroi, L.C.; Lovino, M.A.; Berbery, E.H.; Müller, G.V. Characteristics of droughts in Argentina’s core crop region. *Hydrol. Earth Syst. Sci.* **2021**, *25*, 2475–2490. [[CrossRef](#)]
30. Wu, M.; Vico, G.; Manzoni, S.; Cai, Z.; Bassiouni, M.; Tian, F.; Zhang, J.; Ye, K.; Messori, G. Early Growing Season Anomalies in Vegetation Activity Determine the Large-Scale Climate-Vegetation Coupling in Europe. *J. Geophys. Res. Biogeosciences* **2021**, *126*. [[CrossRef](#)]
31. Parinussa, R.M.; Wang, G.; Liu, Y.; Lou, D.; Hagan, D.F.T.; Zhan, M.; Su, B.; Jiang, T. Improved surface soil moisture anomalies from Fengyun-3B over the Jiangxi province of the People’s Republic of China. *Int. J. Remote Sens.* **2018**, *39*, 8950–8962. [[CrossRef](#)]
32. Otkin, J.A.; Zhong, Y.; Lorenz, D.; Anderson, M.C.; Hain, C. Exploring seasonal and regional relationships between the Evaporative Stress Index and surface weather and soil moisture anomalies across the United States. *Hydrol. Earth Syst. Sci.* **2018**, *22*, 5373–5386. [[CrossRef](#)]
33. Lorenz, D.J.; Otkin, J.A.; Svoboda, M.; Hain, C.R.; Anderson, M.C.; Zhong, Y. Predicting U.S. Drought Monitor States Using Precipitation, Soil Moisture, and Evapotranspiration Anomalies. Part I: Development of a Nondiscrete USDM Index. *J. Hydrometeorol.* **2017**, *18*, 1943–1962. [[CrossRef](#)]
34. Lorenz, D.J.; Otkin, J.A.; Svoboda, M.; Hain, C.R.; Anderson, M.C.; Zhong, Y. Predicting the U.S. Drought Monitor Using Precipitation, Soil Moisture, and Evapotranspiration Anomalies. Part II: Intraseasonal Drought Intensification Forecasts. *J. Hydrometeorol.* **2017**, *18*, 1963–1982. [[CrossRef](#)]
35. DU, L.; Tian, Q.; Yu, T.; Meng, Q.; Jancsó, T.; Udvardy, P.; Huang, Y. A comprehensive drought monitoring method integrating MODIS and TRMM data. *Int. J. Appl. Earth Obs. Geoinf.* **2013**, *23*, 245–253. [[CrossRef](#)]
36. Zhang, X.; Chen, N.; Li, J.; Chen, Z.; Niyogi, D. Multi-sensor integrated framework and index for agricultural drought monitoring. *Remote Sens. Environ.* **2017**, *188*, 141–163. [[CrossRef](#)]
37. Liu, Q.; Zhang, S.; Zhang, H.; Bai, Y.; Zhang, J. Monitoring drought using composite drought indices based on remote sensing. *Sci. Total. Environ.* **2020**, *711*, 134585. [[CrossRef](#)] [[PubMed](#)]
38. Wei, W.; Zhang, J.; Zhou, J.; Zhou, L.; Xie, B.; Li, C. Monitoring drought dynamics in China using Optimized Meteorological Drought Index (OMDI) based on remote sensing data sets. *J. Environ. Manag.* **2021**, *292*, 112733. [[CrossRef](#)] [[PubMed](#)]
39. Wei, W.; Zhang, H.Y.; Zhou, J.J.; Zhou, L.; Xie, B.B.; Li, C.H. Drought monitoring in arid and semi-arid region based on mul-ti-satellite datasets in northwest, China. *Environ. Sci. Pollut.* **2021**, *28*, 51556–51574. [[CrossRef](#)] [[PubMed](#)]
40. Niu, N.; Li, J. Interannual variability of autumn precipitation over South China and its relation to atmospheric circulation and SST anomalies. *Adv. Atmos. Sci.* **2008**, *25*, 117–125. [[CrossRef](#)]
41. Zhang, W.; Jin, F.-F.; Turner, A. Increasing autumn drought over southern China associated with ENSO regime shift. *Geophys. Res. Lett.* **2014**, *41*, 4020–4026. [[CrossRef](#)]
42. Zhang, W.; Jin, F.-F.; Zhao, J.-X.; Qi, L.; Ren, H.-L. The Possible Influence of a Nonconventional El Niño on the Severe Autumn Drought of 2009 in Southwest China. *J. Clim.* **2013**, *26*, 8392–8405. [[CrossRef](#)]
43. Wang, P.; Tam, C.-Y.; Xu, K. El Niño–East Asian monsoon teleconnection and its diversity in CMIP5 models. *Clim. Dyn.* **2019**, *53*, 6417–6435. [[CrossRef](#)]
44. Pei, F.; Zhou, Y.; Xia, Y. Application of Normalized Difference Vegetation Index (NDVI) for the Detection of Extreme Precipitation Change. *Forests* **2021**, *12*, 594. [[CrossRef](#)]
45. Zhang, D.Q.; Chen, L.J. Possible mechanisms for persistent anomalous rainfall over the middle and lower reaches of Yangtze River in winter 2018/2019. *Int. J. Climatol.* **2021**. [[CrossRef](#)]

46. Chen, Y.; Huang, J.; Sheng, S.; Mansaray, L.R.; Liu, Z.; Wu, H.; Wang, X. A new downscaling-integration framework for high-resolution monthly precipitation estimates: Combining rain gauge observations, satellite-derived precipitation data and geographical ancillary data. *Remote Sens. Environ.* **2018**, *214*, 154–172. [[CrossRef](#)]
47. Rodell, M.; Houser, P.R.; Jambor, U.; Gottschalck, J.; Mitchell, K.; Meng, C.-J.; Arsenault, K.; Cosgrove, B.; Radakovich, J.; Bosilovich, M.; et al. The Global Land Data Assimilation System. *Bull. Am. Meteorol. Soc.* **2004**, *85*, 381–394. [[CrossRef](#)]
48. Chen, Y.; Yang, K.; Qin, J.; Zhao, L.; Tang, W.; Han, M. Evaluation of AMSR-E retrievals and GLDAS simulations against observations of a soil moisture network on the central Tibetan Plateau. *J. Geophys. Res. Atmos.* **2013**, *118*, 4466–4475. [[CrossRef](#)]
49. Liu, L.; Huang, J.; Xiong, Q.; Zhang, H.; Song, P.; Huang, Y.; Dou, Y.; Wang, X. Optimal MODIS data processing for accurate multi-year paddy rice area mapping in China. *GIScience Remote Sens.* **2020**, *57*, 687–703. [[CrossRef](#)]
50. Chen, Y.; Lu, D.; Moran, E.; Batistella, M.; Dutra, L.V.; Sanches, I.D.; da Silva, R.F.B.; Huang, J.; Luiz, A.J.B.; de Oliveira, M.A.F. Mapping croplands, cropping patterns, and crop types using MODIS time-series data. *Int. J. Appl. Earth Obs. Geoinf.* **2018**, *69*, 133–147. [[CrossRef](#)]
51. Chen, Y.Y. Risk Assessment and Monitoring of Winter Wheat Waterlogging Combining Ground-Based Observations and Satellite-Derived Data. Ph.D. Thesis, Zhejiang University, Hangzhou, China, 2018. (In Chinese).
52. Boschetti, M.; Busetto, L.; Manfron, G.; Laborte, A.; Asilo, S.; Pazhanivelan, S.; Nelson, A. PhenoRice: A method for automatic extraction of spatio-temporal information on rice crops using satellite data time series. *Remote Sens. Environ.* **2017**, *194*, 347–365. [[CrossRef](#)]
53. Xu, K.; Miao, H.; Liu, B.; Tam, C.; Wang, W. Aggravation of Record-Breaking Drought over the Mid-to-Lower Reaches of the Yangtze River in the Post-monsoon Season of 2019 by Anomalous Indo-Pacific Oceanic Conditions. *Geophys. Res. Lett.* **2020**, *47*. [[CrossRef](#)]
54. Rajsekhar, D.; Singh, V.P.; Mishra, A.K. Multivariate drought index: An information theory based approach for integrated drought assessment. *J. Hydrol.* **2015**, *526*, 164–182. [[CrossRef](#)]
55. Cardil, A.; Vega-Garcia, C.; Ascoli, D.; Molina-Terren, D.; Silva, C.; Rodrigues, M. How does drought impact burned area in Mediterranean vegetation communities? *Sci. Total. Environ.* **2019**, *693*, 133603. [[CrossRef](#)] [[PubMed](#)]
56. Anderson, M.; Zolin, C.A.; Sentelhas, P.C.; Hain, C.R.; Semmens, K.; Yilmaz, M.T.; Gao, F.; Otkin, J.; Tetrault, R. The Evaporative Stress Index as an indicator of agricultural drought in Brazil: An assessment based on crop yield impacts. *Remote Sens. Environ.* **2016**, *174*, 82–99. [[CrossRef](#)]
57. Niyogi, D.; Liu, X.; Andresen, J.; Song, Y.; Jain, A.K.; Kellner, O.; Takle, E.S.; Doering, O.C. Crop models capture the impacts of climate variability on corn yield. *Geophys. Res. Lett.* **2015**, *42*, 3356–3363. [[CrossRef](#)]